Proteolytic cleavage and inactivation of the TRMT1 tRNA modification enzyme by SARS-CoV-2 main protease

Kejia Zhang[a], Jessica H. Ciesla[b], Patrick Eldin[c], Laurence Briant[c], Jenna M. Lentini[a], Jillian Ramos[a], Joshua Munger[b], and Dragony Fu[a*]

[a] Department of Biology, Center for RNA Biology, University of Rochester, Rochester, NY, 14627, USA

[b] Department of Biochemistry and Biophysics, University of Rochester Medical Center, Rochester, NY 14642, USA

[c] Institut de Recherche en Infectiologie de Montpellier (IRIM), CNRS, UMR 9004, Université de Montpellier, 1919 Route de Mende, 34293, Montpellier Cedex 5, France.

* Corresponding author:

dragonyfu@rochester.edu

Keywords: SARS-CoV-2, coronavirus, Nsp5, main protease, 3CLpro, Mpro, TRMT1, tRNA modification, methyltransferase

ABSTRACT

Nonstructural protein 5 (Nsp5) is the main protease of SARS-CoV-2 that cleaves viral polyproteins into individual polypeptides necessary for viral replication. Here, we show that Nsp5 binds and cleaves human tRNA methyltransferase 1 (TRMT1), a host enzyme required for a common post-transcriptional modification in tRNAs. Human cells infected with SARS-CoV-2 exhibit a decrease in TRMT1 protein levels and TRMT1-catalyzed tRNA modifications, consistent with TRMT1 cleavage and inactivation by Nsp5. Nsp5 cleaves TRMT1 at a specific position that matches the consensus sequence of SARS-CoV-2 polyprotein cleavage sites, and a single mutation within the sequence inhibits Nsp5-dependent proteolysis of TRMT1. The TRMT1 cleavage fragments exhibit altered RNA binding activity and are unable to rescue tRNA modification in TRMT1-deficient human cells. Compared to wildtype human cells, TRMT1-deficient human cells infected with SARS-CoV-2 exhibit reduced levels of intracellular viral RNA. These findings suggest that Nsp5-dependent cleavage of TRMT1 and perturbation of tRNA modification patterns contribute to the cellular pathogenesis and biology of SARS-CoV-2 infection.

INTRODUCTION

Severe acute respiratory syndrome coronavirus 2 (SARS-CoV-2) is an enveloped, single-stranded RNA virus that is the causative agent of the COVID-19 pandemic (Lamers & Haagmans, 2022; Merad *et al*, 2022). SARS-CoV-2 is a member of the Betacoronavirus genus of the Coronaviridae family, which includes the severe acute respiratory syndrome coronavirus 1 (SARS-CoV-1) and Middle East respiratory syndrome coronavirus (MERS-CoV). SARS-CoV-2 primarily targets the human respiratory tract and lungs, which can clinically manifest as an acute respiratory distress syndrome. Once delivered into the host cell, the incoming positive-strand viral RNA genome is first translated by host ribosomes into two overlapping polyproteins, pp1a and pp1ab. Viral polyproteins are then proteolytically processed into 16 mature nonstructural proteins (Nsps) involved in the assembly of the viral replication-transcription complex (reviewed in (V'Kovski *et al*, 2021)).

The maturation step to release the individual Nsp polypeptides is executed by two viral-encoded proteases: Nsp5 (also known as Main Protease, M^{Pro}/3C-like protease) and Nsp3 (also known as Papain-Like Protease, PL^{Pro}) (Narayanan *et al*, 2022). Nsp3 cleaves pp1a to release Nsp1 through Nsp4, including auto-processing cites for self-cleavage (Yan & Wu, 2021). The Nsp5 main protease processes pp1b at eleven sites to release itself and Nsp4 to Nsp16 (Chen *et al*, 2021). Besides cleaving viral substrates, Nsp3 and Nsp5 have also been found to cleave endogenous host proteins linked to the immune response and cell survival (Liu *et al*, 2021; Meyer *et al*, 2021; Meyers *et al*, 2021; Moustaqil *et al*, 2021; Wenzel *et al*, 2021; Zhang *et al*, 2021b). Nsp3 and Nsp5 are essential for viral replication and represent well-characterized drug targets among coronaviruses. Notably, the active component of the antiviral drug Paxlovid is nirmatrelvir, a reversible covalent inhibitor of the Nsp5 main protease (Owen *et al*, 2021). By inhibiting Nsp5 proteolytic activity, Paxlovid reduces viral replication and disease severity in patients with COVID-19.

Purification of individual SARS-CoV-2 proteins from human cells have identified a potential interaction between a catalytic-inactive version of Nsp5 with human tRNA methyltransferase 1 (TRMT1) (Gordon *et al*, 2020b). A cross-coronavirus investigation from the same group has extended this observation by finding that TRMT1 interacts with a catalytic-inactive version of Nsp5 encoded by SARS-CoV-1, which is 98.7% similar to SARS-CoV-2 (Gordon *et al*, 2020a). Interestingly, the same study found no detectable interaction between TRMT1 and Nsp5 encoded by MERS-CoV, which has 66.8% similarity with SARS-CoV-2. In an independent study, TRMT1 was also identified as a potential interactor with catalytic-inactive Nsp5 using proximity-dependent biotinylation (Samavarchi-Tehrani *et al*, 2020).

TRMT1 is a tRNA modification enzyme that catalyzes the formation of dimethylguanosine (m2,2G) at position 26 in more than half of all human tRNAs (Dewe *et al*, 2017; Jonkhout *et al*, 2021). The m2,2G modification is located at a key structural position in tRNAs and is hypothesized to play a role in proper tRNA folding (Pallan *et al*, 2008; Steinberg & Cedergren, 1995). TRMT1-deficient human cells exhibit perturbations in global protein synthesis and decreased proliferation (Dewe *et al.*, 2017).

Moreover, loss-of-function variants in the *TRMT1* gene are the cause of certain types of intellectual disability disorders in humans (Blaesius *et al*, 2018; Najmabadi *et al*, 2011; Zhang *et al*, 2020b). Thus, changes in TRMT1 activity can impact protein synthesis leading to downstream cellular and biological effects.

The putative interaction between Nsp5 and TRMT1 indicates that SARS-CoV-2 infection could affect the levels or function of TRMT1. However, the association between Nsp5 and TRMT1 has not been validated nor characterized. Here, we find that TRMT1 is an endogenous cleavage target of Nsp5 resulting in methyltransferase inactive cleavage products. Moreover, we find that SARS-CoV-2 infection correlates with decreased TRMT1 levels and a reduction in m2,2G-modified tRNAs. In addition, we provide evidence that TRMT1 expression is required for efficient SARS-CoV-2 replication in human cells. These studies uncover TRMT1 as a novel proteolytic cleavage target of Nsp5 during SARS-CoV-2 infection and suggest possible pathological mechanisms associated with perturbations in TRMT1-catalyzed tRNA modifications.

RESULTS

SARS-CoV-2 infection reduces cellular levels of TRMT1 and TRMT1-catalyzed tRNA modifications

To test the effects of SARS-CoV-2 infection on TRMT1 and tRNA modifications, we used a MRC-5 human lung fibroblast cell line expressing the ACE2 receptor that is permissive for SARS-CoV-2 infection (Raymonda *et al*, 2022; Uemura *et al*, 2021a; Uemura *et al*, 2021b). MRC-5 cells were mock-infected or infected with SARS-CoV-2 followed by harvesting at 24- and 48-hours post-infection for sample preparation. Immunoblotting for the SARS-CoV-2 nucleocapsid (N) protein confirmed the infection and expression of viral proteins in MRC-5 cells compared to mock infected cells (Figure 1A, N protein, compare lanes 1 and 2 to lanes 3 and 4). To probe for TRMT1, we used an antibody that detects the major TRMT1 isoform of ~72 kDa as well as a non-specific band at ~65 kDa in human cell lysates (Dewe *et al.*, 2017; Perez *et al*, 2022). Using this antibody, we also detected the 72 kDa TRMT1 isoform

as well as the non-specific 65 kDa band in MRC-5 cell lysates (Figure 1A, circle denotes TRMT1, asterisk denotes non-specific band). In multiple independent replicates, MRC-5 cells infected with SARS-CoV-2 exhibited a ~30% reduction in TRMT1 levels at 24- and 48-hours post-infection compared to mock-infected cells (Representative blot shown in Figure 1A, quantified in 1B). No lower molecular weight TRMT1 cleavage products were detectable in lysates prepared from the MRC-5 cells infected with SARS-CoV-2. The lack of detectable TRMT1 cleavage products could be due to the low basal levels of TRMT1 in MRC-5 cells and/or degradation of the TRMT1 cleavage products in SARS-CoV-2-infected cells.

We next measured the levels of TRMT1-catalyzed m2,2G modifications in cellular RNA using quantitative mass spectrometry (Zhang *et al*, 2020a). While m2,2G levels did not exhibit a significant change between mock-infected and SARS-CoV-2-infected cells at 24 hours post-infection, m2,2G levels were decreased by ~15% at 48 hours post-infection (Figure 1C). In addition to m2,2G, more than half of all tested RNA modifications exhibited a decrease in SARS-CoV-2-infected cells compared to mock-infected cells at 24 hours post-infection (Figure 1D). At 48 hours post-infection with SARS-CoV-2, most of the tested RNA modifications exhibited a decrease in levels compared to mock-infected cells. Thus, SARS-CoV-2 infection of human MRC-5 lung fibroblast cells alters the steady-state levels of multiple tRNA modifications, including the m2,2G modification catalyzed by TRMT1.

Nsp5 binds and cleaves TRMT1 in a site-specific manner

Examination of the primary structure of human TRMT1 revealed an eight amino acid residue sequence between the methyltransferase domain and zinc-finger motif matching the consensus sequence of Nsp5 cleavage sites in SARS-CoV-2 polyproteins (Figure 2A, B). The putative cleavage site in TRMT1 includes a glutamine (Q) residue conserved at the fourth position that is found in all Nsp5 cleavage sites of SARS-CoV-2 polyproteins (Figure 2B). Based upon a predicted tertiary structure of TRMT1 using Alpha Fold (Jumper *et al*, 2021; Varadi *et al*, 2022), this putative Nsp5 cleavage site is expected to lie in an unstructured linker region exposed on the surface of TRMT1 (Figure 2C).

To investigate a potential interaction between Nsp5 and TRMT1, we used human 293T cells due to their high transfection efficiency. We transfected human 293T cells with plasmids expressing wildtype (WT) Nsp5 from SARS-CoV-2 or Nsp5-C145A. The Nsp5-C145A mutant contains an alanine substitution of the catalytic cysteine residue in the active site of Nsp5 and is proteolytically inactive (Lee *et al*, 2020). The Nsp5 proteins were expressed as fusion proteins with the Twin-Strep purification tag (Schmidt *et al*, 2013). We also tested the interaction between Strep-Nsp5 or Nsp5-C145A with TRMT1 by co-expression with FLAG-tagged TRMT1. The Strep-tagged Nsp5 or Nsp5-C145A mutant were affinity purified from cell lysates on streptactin resin, eluted with biotin and purified proteins detected by immunoblotting. Probing of input lysates and purified samples with anti-Strep antibodies confirmed the expression and recovery of WT-Nsp5 and Nsp5-C145A (Figure 2D, Strep). To probe for TRMT1, we used the antibody described above that detects endogenous full-length TRMT1 of 72 kDa (Figure 2D, input lanes 1 to 3, circle denotes endogenous TRMT1). The antibody also detected the overexpressed TRMT1-FLAG protein (Figure 2D, lanes 4 to 6, square denotes TRMT1-FLAG). Only background levels of endogenous TRMT1 or TRMT1-FLAG were detected in the vector or WT-Nsp5 purifications (Figure 2D, TRMT1, low or high exposure, lanes 7, 8, 10 and 11). In contrast, endogenous TRMT1 was enriched in the purification with Nsp5-C145A (Figure 2D, TRMT1 high exposure, lane 9). TRMT1-FLAG was also detected specifically in the Nsp5-C145A purification compared to the control or Nsp5 purifications (Figure 2D, compare lanes 10 and 11 to lane 12).

The interaction of TRMT1 with Nsp5-C145A along with cleavage site prediction suggests that TRMT1 could be a proteolysis substrate of Nsp5. To test this hypothesis, we monitored for TRMT1 cleavage in 293T human cells expressing Strep-Nsp5 or Strep-GFP as a control. Cleavage after amino acid residue 530 of TRMT1 is predicted to result in an N-terminal fragment of 58 kDa and a C-terminal fragment of 14 kDa. To probe for the N-terminal TRMT1 fragment, we used the antibody described above which targets residues 201 to 229 of TRMT1. Using this antibody, we detected full-length TRMT1 and the ~65 kDa non-specific band in lysates from 293T cells expressing Strep-GFP (Figure 2E, TRMT1, lanes 1 to 3, circle and asterisk, respectively). Notably, lysates prepared from human cells expressing

Nsp5 exhibited an additional band migrating below the non-specific band that matches the predicted size of the N-terminal TRMT1 fragment (Figure 2E, TRMT1, lanes 4 to 6, arrow). The putative N-terminal TRMT1 fragment was detectable at 24 hours post-transfection with the Nsp5-expression plasmid, increased at 48 hours, and remained detectable at 72 hours post-transfection (Figure 2E). In contrast, the N-terminal TRMT1 fragment was not detected above background signal in human cells expressing the proteolytically inactive Nsp5-C145A mutant (Figure 2E, TRMT1, lanes 7 to 9, quantified in 2F). We also validated the specificity of our results by using a human 293T TRMT1-knockout (KO) cell line that is deficient in TRMT1 expression (Dewe *et al.*, 2017; Zhang *et al.*, 2020a). In this case, neither full-length TRMT1 nor the TRMT1 cleavage fragment were detected in a TRMT1-deficient human cell line expressing Nsp5 (Figure 2G, compare lanes 1 through 3 to lanes 4 through 6). This result provides additional confirmation that the N-terminal TRMT1 fragment arises from cleavage of endogenous TRMT1 by Nsp5.

We also attempted to detect the C-terminal TRMT1 cleavage fragment in human cells expressing Nsp5 using an antibody targeting residues 609 to 659 of TRMT1 (Zhang *et al*, 2021a). This anti-TRMT1 antibody detects the full-length 72 kDa TRMT1 isoform that is absent in TRMT1-KO cells (Supplemental Figure 1A, lanes 1 and 2). However, no additional band matching the expected size of the C-terminal fragment was detected in human cells expressing Nsp5 compared to cells expressing GFP or Nsp5-C145A (Supplemental Figure 1A, lanes 3 through 6). This could be due to degradation of the C-terminal TRMT1 fragment and/or low sensitivity of the antibody.

To increase the sensitivity for detecting the C-terminal TRMT1 fragment, we co-transfected Nsp5 expression plasmids along with a plasmid encoding TRMT1 fused to a FLAG tag at the C-terminus. Confirming the results above with endogenous TRMT1, the N-terminal TRMT1 cleavage product was detected in the lysate of human cells overexpressing TRMT1-FLAG and Nsp5 but not with vector or Nsp5-C145A (Figure 3A, TRMT1, compare lanes 1 and 3 to lane 2). In addition, using an antibody against the FLAG tag, we could detect a ~20 kDa product matching the expected molecular weight of a FLAG-tagged C-terminal TRMT1 cleavage product in the lysate of human cells expressing Nsp5 but not

vector alone or Nsp5-C145A (Figure 3A, FLAG, arrowhead). To confirm that the 20 kDa band detected with the anti-FLAG antibody was the C-terminal portion of TRMT1, we probed the cell lysates with the anti-TRMT1 antibody targeting residues 609 to 659 noted above. Using this antibody, we detected the same ~20 kDa band in the lysate of human cells expressing Nsp5 but not vector alone or Nsp5-C145A (Supplemental Figure 1B, lanes 1 to 3). These data provide evidence that SARS-CoV-2 Nsp5 cleaves at the predicted cleavage site in TRMT1 leading to N- and C-terminal fragments in human cells.

All Nsp5 cleavage sites in SARS-CoV-1 and SARS-CoV-2 polyproteins contain a glutamine residue at position four (Grum-Tokars *et al*, 2008; Jin *et al*, 2022; Lee *et al*, 2022). Mutation of the glutamine to asparagine is sufficient to abolish recognition and cleavage by Nsp5 from SARS-CoV-1 or SARS-CoV-2 (Heilmann *et al*, 2022; Muramatsu *et al*, 2013). Thus, we tested if TRMT1 exhibited the same requirements for cleavage by Nsp5 by generating an expression construct for TRMT1-FLAG in which residue Q530 of the predicted Nsp5 cleavage site was mutated to asparagine (Figure 3B, Q530N). Further confirming our results above, expression of TRMT1-FLAG with WT-Nsp5 but not GFP or Nsp5-C145A led to the accumulation of N- and C-terminal TRMT1 cleavage fragments (Figure 3C, TRMT1 and FLAG, lanes 4 to 6, arrow and arrowhead, Supplemental Figure 1B). In contrast to wildtype TRMT1, the appearance of the N- or C-terminal TRMT1 cleavage fragments was barely detectable when the TRMT1-Q530N mutant was co-expressed with Nsp5 (Figure 3C, lane 8, Supplemental Figure 1B). Altogether, these results demonstrate that TRMT1 can be recognized and cleaved by Nsp5 in human cells with cleavage requiring a sequence that matches Nsp5 cleavage sites in SARS-CoV-2 polyproteins.

Functional properties of TRMT1 fragments resulting from Nsp5 cleavage

Cleavage of TRMT1 after residue Q530 will result in an N-terminal fragment encompassing the methyltransferase domain and a C-terminal TRMT1 fragment containing a zinc finger motif that mediates tRNA interaction (Dewe *et al.*, 2017; Zhang *et al.*, 2020a). Thus, we tested the functional properties of the predicted TRMT1 cleavage fragments compared to full-length TRMT1. First, we tested the interaction between the TRMT1 cleavage fragments and RNA. We have previously shown that TRMT1 exhibits a

stable interaction with rRNAs and substrate tRNAs that are targets for m2,2G modification (Dewe *et al.*, 2017; Zhang *et al.*, 2020a). Based upon this interaction, we expressed full-length TRMT1, the TRMT1-Q530N mutant, or the TRMT1 fragments as FLAG-tagged fusion proteins in 293T human cells followed by affinity purification and analysis of copurifying RNAs (Figure 4A). Immunoblotting confirmed the expression and purification of each TRMT1 variant on anti-FLAG resin (Figure 4B). As expected, the purification of full-length TRMT1 resulted in the enrichment of rRNA and tRNAs compared to the control purification from vector-transfected cells (Figure 4C, compare lane 6 to lane 7). The Q530N variant of TRMT1 also exhibited comparable binding of tRNAs as full-length TRMT1 (Figure 4C, lane 10). In contrast, no detectable enrichment of rRNA or tRNA was detected for the N-terminal TRMT1 fragment (Figure 4C, lane 8). Interestingly, the TRMT1 C-terminal fragment exhibited similar levels of tRNA binding as full-length TRMT1 (Figure 4C, compare lane 7 to 9). Thus, the N-terminal TRMT1 cleavage fragment appears to be defective in binding tRNA while the C-terminal fragment containing the Zn-finger motif is sufficient for binding to tRNAs.

To further dissect the functionality of the TRMT1 cleavage fragments, we next used the TRMT1-KO human cell line described above. This TRMT1-KO cell line is deficient in TRMT1 and lacks m2,2G modifications in all tested tRNAs containing G at position 26 (Dewe *et al.*, 2017; Zhang *et al.*, 2020a). Using transient transfection, we expressed full-length TRMT1 or the TRMT1 variants in either the control wildtype (WT) or TRMT1-KO cell lines (Figure 4D). We then assessed for rescue of m2,2G formation in nuclear-encoded tRNA-Met-CAU or mitochondrial-encoded (mt)-tRNA-Ile-UAU using a reverse transcriptase (RT)-based primer extension assay. Based upon this assay, vector-transfected WT human cells exhibited an RT block at position 26 of tRNA-Met-CAU and mt-tRNA-Ile-UAU indicative of the m2,2G modification (Figure 4E, Lane 1). No read-through product was detected for either tRNA in control human cells indicating that nearly all endogenous tRNA-Met-CAU and mt-tRNA-Ile-UAU is modified with m2,2G. Consistent with this observation, increased expression of full-length TRMT1 or variants in control 239T cells had no detectable effect on m2,2G modification in tRNA-Met-CAU or mt-tRNA-Ile-UAU (Figure 4E, lanes 2 through 5).

As expected, the m2,2G modification was absent in tRNA-Met-CAU and mt-tRNA-Ile-UAU isolated from the vector-transfected TRMT1-KO cell line leading to read-through to the next RT block (Figure 4E, lane 6). Re-expression of full-length TRMT1 or TRMT1-Q530N in the TRMT1-KO cell line was able to restore m2,2G formation in both tRNA-Met-CAU and mt-tRNA-Ile-UAU (Figure 4E, lanes 7 and 9). However, neither the N- nor C-terminal TRMT1 fragment was able to restore m2,2G formation in the tRNAs of the TRMT1-KO cell line (Figure 4E, lanes 8 and 10). These results indicate that cleavage of TRMT1 by Nsp5 leads to protein fragments that are inactive for tRNA modification activity.

TRMT1-deficient human cells exhibit reduced levels of SARS-CoV-2 RNA replication

We next investigated whether TRMT1 expression impacts SARS-CoV-2 replication by infecting the 293T wildtype or TRMT1-KO human cell lines described above. To render the 293T cell lines permissive for SARS-CoV-2 infection, the cell lines were engineered to stably express the ACE2 receptor from an integrated lentiviral vector (Figure 5A). The ACE2-expressing cell lines were infected at low or high multiplicity of infection (MOI) followed by harvesting of cells at 24 hours post-infection to monitor intracellular viral RNA levels by quantitative RT-PCR. As expected, titration of SARS-CoV-2 viral particles at either low or high MOI led to a concomitant increase in viral RNA in both control and TRMT1-KO cell lines (Figure 5B and C). However, TRMT1-KO cells exhibited a ~3 to 4-fold reduction in viral RNA compared to control cells infected at the same MOI (Figure 5B and C). These results suggest that expression of TRMT1 is necessary for efficient SARS-CoV-2 replication in human cells.

DISCUSSION

Here, we show that human TRMT1 is cleaved at a specific position by the SARS-CoV-2 Nsp5 main protease to produce methyltransferase-inactive fragments. In addition, we demonstrate that TRMT1 protein and TRMT1-catalyzed tRNA modifications are reduced in human cells infected with SARS-CoV-2. TRMT1 could represent a coincidental substrate of Nsp5 during SARS-CoV-2 infection due to the presence of a sequence matching the cleavage site of SARS-CoV-2 polyproteins. Since the majority of

TRMT1 exhibits steady-state localization to the nucleus and mitochondria of multiple human cell types (Dewe *et al.*, 2017), Nsp5 could have access mainly to newly synthesized TRMT1 in the cytoplasm. Moreover, the effect of SARS-CoV-2 infection on TRMT1 levels could depend on the concentration of TRMT1, half-life of TRMT1, and/or amount of Nsp5 expression in the infected cell. This could account for the observation that TRMT1 levels are reduced but not abolished in human cells infected with SARS-CoV-2. Consistent with our results, a subset of proteomic studies has found decreased TRMT1 protein levels in SARS-CoV-2-infected human cells as well as in post-mortem tissue samples from decreased COVID-19 patients (Bojkova *et al*, 2020; Nie *et al*, 2021). These findings suggest that SARS-CoV-2 infection could impact TRMT1 protein levels and tRNA modification patterns within the cells of an infected individual.

While TRMT1 cleavage could be a collateral effect of SARS-CoV-2 infection, the subsequent impact on tRNA modification levels could have physiological consequences on downstream molecular processes that ultimately affect cellular health and/or viral replication. We have previously shown that TRMT1-deficient human cells exhibit decreased levels of global protein synthesis, perturbations in redox metabolism, and reduced proliferation (Dewe *et al.*, 2017). Moreover, we have found that partial depletion of TRMT1 is sufficient to increase the oxidative stress sensitivity of human neural stem cells. Thus, the reduction in TRMT1 and TRMT1-catalyzed tRNA modifications observed in human lung cells upon SARS-CoV-2 infection could lead to changes in protein synthesis that affects cellular proliferation and metabolism. In lung tissues, the disruption of TRMT1-dependent processes caused by changes in TRMT1-catalyzed tRNA modification levels could contribute to the pathophysiological outcomes associated with COVID-19 disease. Consistent with this possibility, TRMT1 has been identified as a prognosis factor for SARS-CoV-2 disease severity (Li *et al*, 2021a).

Notably, we have found that human cells deficient in TRMT1 display reduced viral RNA levels compared to wildtype cells after SARS-CoV-2 infection. This finding suggests that TRMT1 expression is required for efficient SARS-CoV-2 replication and that TRMT1 cleavage by Nsp5 could be inhibitory for viral RNA synthesis. As mentioned above, TRMT1-deficient human cells exhibit an overall reduction in

global protein synthesis due to the loss of m2,2G modifications in tRNAs (Dewe *et al.*, 2017). Thus, the TRMT1-deficient human cells could present a cellular environment that is unable to support the levels of translation necessary for efficient virus production. In addition, TRMT1-deficient human cells could exhibit changes in gene expression and cellular metabolism that are suboptimal for SARS-CoV-2 replication.

While TRMT1 could be an unintentional target of Nsp5, it remains possible that TRMT1 cleavage modulates the SARS-CoV-2 life cycle through an uncharacterized process. One possibility is that viral RNAs could be substrates of TRMT1-catalyzed RNA methylation. Previous studies have found that endogenous host RNA modification enzymes can modify the genomic and sub-genomic RNAs of SARS-CoV-2 (Burgess *et al*, 2021; Di Giorgio *et al*, 2020; Li *et al*, 2021b; Peng *et al*, 2022; Zhang *et al*, 2021c). Moreover, uncharacterized modifications have been identified through Nanopore sequencing in the genomic and subgenomic RNAs of SARS-CoV-2 (Kim *et al*, 2020). There could be portions of the SARS-CoV-2 genome or subgenomic RNAs that fold into substrates that resemble tRNA targets of TRMT1. Moreover, the N-terminal TRMT1 fragment could gain the ability to modify viral RNAs due to altered binding specificity since the N-terminal TRMT1 fragment retains the entire methyltransferase domain but not the Zn-finger motif involved in tRNA interaction. The C-terminal Zn-finger motif itself could also exhibit altered binding specificity and interact with SARS-CoV-2 RNAs. In turn, this could affect the SARS-CoV-2 life cycle such as replication, viral gene expression and infectivity. Future studies will examine for possible interactions between TRMT1 and the SARS-CoV-2 transcriptome as well as the presence of TRMT1-catalyzed modifications in SARS-CoV-2 RNAs.

Experimental Procedures

Cell culture

293T human embryonic cell lines were cultured in Dulbecco's Minimal Essential Medium (DMEM) containing 10% fetal bovine serum, 2 mM L-alanyl-L-glutamine (GlutaMax, Gibco) and 1% Penicillin/Streptomycin. Cells were grown at 37 degrees, 20% Oxygen, and 5% CO_2. Telomerase-

immortalized MRC5 fibroblasts expressing ACE2 (MRC5-ACE2 cells) were cultured in Dulbecco's modified Eagle serum (DMEM; Invitrogen) supplemented with 10% (vol/vol) fetal bovine serum (FBS) (Atlanta Biologicals), 4.5 g/L glucose, and 1% penicillin-streptomycin (Pen-Strep; Life Technologies) at 37 °C in a 5% (vol/vol) CO2 atmosphere. Vero-E6 cells were cultured in Eagle's Minimum Essential Medium (ATCC, #30–2003) supplemented with 10% (vol/vol) fetal bovine serum (FBS) (Atlanta Biologicals), 4.5 g/L glucose, 1X Glutamax (Life Technologies, #35050061), and 1% penicillin-streptomycin (Pen-Strep; Life Technologies, #15140122) at 37 °C in a 5% (vol/vol) CO2 atmosphere.

SARS-CoV-2 infection of human cells for protein and RNA analysis

The SARS-CoV-2 isolate, Hong Kong/VM20001061/2020, was previously isolated from a nasopharyngeal aspirate and throat swab from an adult male patient in Hong Kong and was obtained through BEI resources (NR-52282). Viral stocks of SARS-CoV-2 were propagated in Vero-E6 cells in MEM supplemented with 2% (vol/vol) FBS, 4.5 g/L glucose, 1X Glutamax and 1% penicillin-streptomycin at 37 °C. Viral stock titers were determined by TCID50 analysis in Vero-E6 cells. Experiments involving live SARS-CoV-2 were conducted in a biosafety level 3 facility at the University of Rochester.

For infection, MRC5-ACE2 cells were grown in 6-well plates to 90% confluence in growth medium (MRC5-ACE2: DMEM supplemented with 10% FBS and 1% Pen-Strep). Prior to infection, cells were washed with 1 mL of DMEM supplemented with 2% FBS and 1 % Pen-Strep. For infection, 750 µL of viral master mix (MOI = 5) was added to each well for 1.5 hr. After the adsorption period, medium was removed and replaced with fresh DMEM supplemented with 2% FBS and 1% Pen-Strep. To harvest protein, the cell monolayer was washed with 1 mL cold PBS and cells were scraped into 250 µL disruption buffer (250 mM Tris-HCl Ph 7.4, 10% glycerol, 2% β-mercaptoethanol, 5% SDS). DNA was sheared using a sonication probe and samples were stored at -20 °C. To harvest RNA, medium was removed, and the monolayer was washed with PBS. Cells were collected in 400 µL Trizol and stored at -80 °C.

Liquid chromatography-mass spectrometry of nucleosides

Total RNA was isolated using Trizol RNA extraction. Small RNAs were subsequently purified from total RNA using the Zymo RNA Clean & Concentrator-5 kit. Small RNAs (1 μg) was digested and analyzed by LC-MS as previously described (Cai *et al*, 2015; Dewe *et al.*, 2017; Zhang *et al.*, 2020a). Briefly, ribonucleosides were separated using a Hypersil GOLD C18 Selectivity Column (Thermo Scientific) followed by nucleoside analysis using a Q Exactive Plus Hybrid Quadrupole-Orbitrap. The modification difference ratio was calculated using the m/z intensity values of each modified nucleoside following normalization to the sum of intensity values for the canonical nucleosides; A, U, G and C.

In silico analysis of TRMT1 structure

The Nsp5 cleavage site sequence logo was generated using: https://weblogo.berkeley.edu/logo.cgi The predicted tertiary structure of human TRMT1 (Uniprot Q9NXH9) was determined using AlphaFold. Structural visualization was performed using UCSF Chimera software developed by the Resource for Biocomputing, Visualization, and Informatics at the University of California, San Francisco (Pettersen *et al*, 2004).

Plasmid constructs

The pcDNA3.1-TRMT1-FLAG expression plasmid has been described previously (Dewe *et al.*, 2017). The pcDNA3.1-TRMT1-FLAG-Q530N expression construct was generated by DpnI site-directed mutagenesis. The pcDNA3.1 expression plasmids encoding the N- and C-terminal TRMT1 fragments were generated by PCR cloning. All plasmid constructs were verified by Sanger sequencing and whole plasmid sequencing (SNPsaurus).

Transient transfection, protein purification, and immunoblotting

Transient transfection and cellular extract production were performed as previously described (Fu *et al*, 2010). Briefly, 2.5 x 10^6 293T HEK cells were transiently transfected by calcium phosphate DNA precipitation with 10-20 µg of plasmid DNA. Cells were harvested by trypsinization and washed once with PBS. The cell pellet was resuspended in 500 µL hypotonic lysis buffer (20 mM HEPES, pH 7.9; 2 mM $MgCl_2$; 0.2 mM EGTA, 10% glycerol, 0.1 mM PMSF, 1 mM DTT), incubated on ice for 5 minutes and subjected to three freeze-thaw cycles in liquid nitrogen and 37°C. NaCl was added to extracts to a final concentration of 400 mM. After centrifugation at 14,000 x g for 15 minutes at 4°C, an equal amount of hypotonic lysis buffer with 0.2% NP-40 was added to 500 µL of soluble cellular extract.

For Strep-tag purification, whole cell extract from transiently transfected cells cell lines (1 mg of total protein) was rotated for 2 hours at 4° C in lysis buffer (20 mM HEPES at pH 7.9, 2 mM MgCl2, 0.2 mM EGTA, 10% glycerol, 1 mM DTT, 0.1 mM PMSF, 0.1% NP-40) with 200 mM NaCl. Resin was washed three times using the same buffer followed by protein analysis. Strep-tagged proteins were purified using MagSTREP "type3" XT beads, 5% suspension (IBA Lifesciences) and eluted with desthiobiotin. FLAG-tagged proteins were purified by incubating whole cell lysates from the transfected cell lines with 20 µL of DYKDDDDK-Tag Monoclonal Antibody Magnetic Microbead (Syd Labs) for three hours at 4 °C. Magnetic resin was washed three times in hypotonic lysis buffer with 200 mM NaCl.

Immunoblotting was performed as previously described (Ramos *et al*, 2019). Briefly, cell extracts and purified protein samples were boiled at 95°C for 5 minutes followed by fractionation on NuPAGE Bis-Tris polyacrylamide gels (Thermo Scientific). Separated proteins were transferred to Immobilon FL polyvinylidene difluoride (PVDF) membrane (Millipore) for immunoblotting. Membrane was blocked by Odyssey blocking buffer for 1 hour at room temperature followed by immunoblotting with the following antibodies: mouse monoclonal anti-TRMT1 aa 201-229 (G3, sc-373687, Santa Cruz Biotechnologies), rabbit polyclonal anti-TRMT1 aa 609-659 (Bethyl, A304-205A); anti-Strep-tag II (NC9261069, Thermo Fisher), anti-FLAG epitope tag (L00018; Sigma), Rabbit polyclonal anti-SARS-CoV-2 nucleoprotein N protein (40068-RP01; Sino Biological) and anti-actin (L00003; EMD Millipore). Proteins were detected

using a 1:10,000 dilution of fluorescent IRDye 800CW goat anti-mouse IgG (925-32210; Thermofisher) or IRDye 680RD Goat anti-Mouse IgG Secondary Antibody (925-68070; Li-COR). Immunoblots were scanned using direct infrared fluorescence via the Odyssey system (LI-COR Biosciences).

RNA analysis by primer extension

Total RNA was extracted using TRIzol LS reagent (Invitrogen). RNAs were diluted into formamide load buffer, heated to 95°C for 3 minutes, and fractionated on a 10% polyacrylamide, Tris-Borate-EDTA (TBE) gel containing 7M urea. Sybr Gold nucleic acid staining (Invitrogen) was conducted to identify the RNA pattern. For primer extension analysis, 1.5 µg of total RNA was pre-annealed with 5'-^{32}P-labeled oligonucleotide and 5x hybridization buffer (250 mM Tris, pH 8.5, and 300 mM NaCl) in a total volume of 7 µl. The mixture was heated at 95°C for 3 min followed by slow cooling to 42°C. An equal amount of extension mix consisting of avian myeloblastosis virus reverse transcriptase (Promega), 5x AMV buffer and 40 µM dNTPs was added. The mixture was then incubated at 42°C for 1 hour and loaded on 15% 7M urea denaturing polyacrylamide gel. Gels were exposed on a phosphor screen (GE Healthcare) and scanned on a Bio-Rad personal molecular followed by analysis using NIH ImageJ software. Primer extension oligonucleotide sequences were previously described (Dewe *et al.*, 2017).

Assays for viral replication

The SARS-CoV-2 was a French Ile de France isolate (www.european-virus-archive.com/virus/sars-cov-2-isolate-betacovfranceidf03722020). Viral stocks were generated by amplification on VeroE6 cells. The supernatant was collected, filtered through a 0.45 µm membrane, and tittered using a TCID50 assay. For infections, the cells were previously transduced with a Lentiviral vector expressing ACE2 using the lentiviral construct RRL.sin.cPPT.SFFV/Ace2.WPRE (MT136) kindly provided by Caroline Goujon (Addgene plasmid # 145842; http://n2t.net/addgene:145842; RRID: Addgene145842) (Ref PMID: 33514628). 72 hours after transduction, accurate ACE2 expression was

controlled on western blot probed with anti-ACE2 antibody (Human ACE-2 Antibody, AF933, R&D systems). ACE2-positive cells (70-80% confluence) were then infected with SARS-CoV-2 diluted to achieve the desired MOI. After 24 hours in culture, the cells were lysed with the Luna® cell ready lysis module (New England Biolabs). The amplification reaction was run on LightcyclerR 480 thermocycler (Roche Diagnostics) using the Luna® Universal One-Step RT-qPCR kit (New England Biolabs), and SARS_For: 5'-ACAGGTACGTTAATAGTTAATAGCGT; SARS_Rev: 5'-ATATTGCAGCAGTACGCACACA; GAPDH_For: 5'-GCTCACCGGCATGGCCTTTCGCGT and GAPDH_Rev: 5'-TGGAGGAGTGGGTGTCGCTGTTGA primers. Each qPCR was performed in triplicate, and the means and standard deviations were calculated. Relative quantification of data obtained from RT-qPCR was used to determine changes in SARS-CoV-2 gene expression across multiple samples after normalization to the internal reference GAPDH gene.

Acknowledgements

The research in this manuscript was supported by NIH T32 Training Grants GM068411 and AI1049815 to J.C.; the Montpellier University of Excellence (ANR-16-IDEX-0006) program to P.E. and L.B.; NIH AI127370 and AI50698 to J.M.; and NSF RAPID 2033354 and NIH GR530882 to D.F. We thank members of the Fu and Ghaemmaghami Labs for comments on this manuscript; the Mass Spectrometry Resource Lab at the University of Rochester; and the Clinical Proteomics Platform, CHU Montpellier.

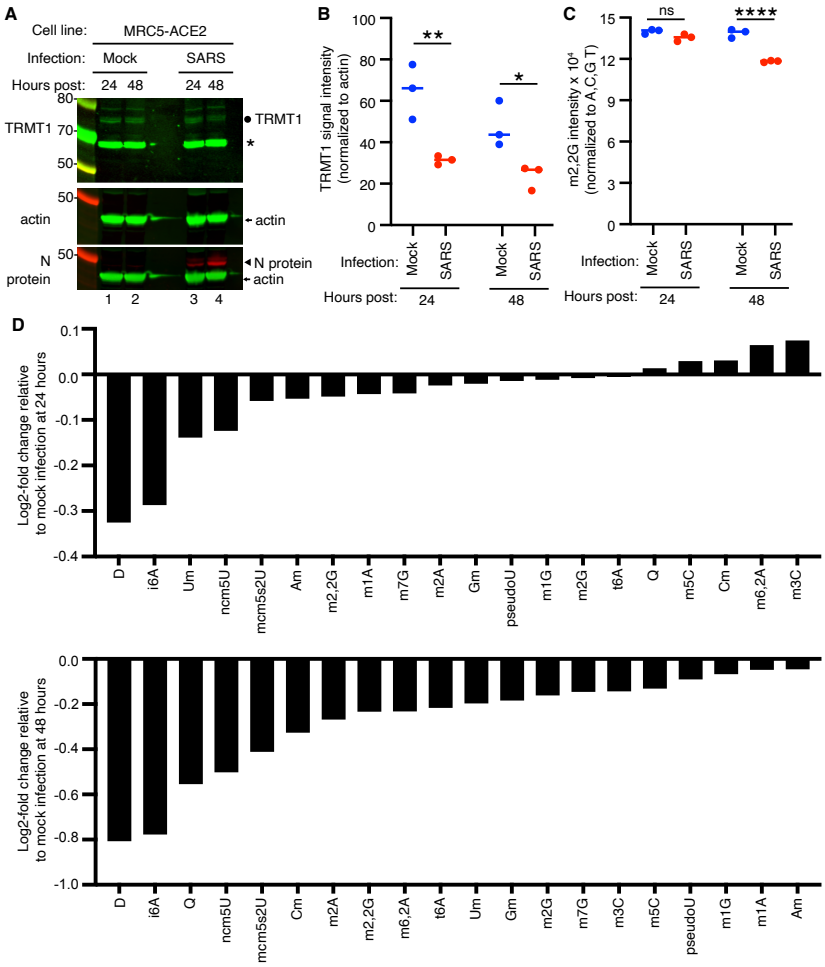

Figure 1. Human cells infected with SARS-CoV-2 exhibit a reduction in TRMT1 levels and perturbations in tRNA modification patterns. (A) Immunoblot analysis of lysates prepared from MRC-5-ACE2 human cells that were mock-infected or infected with SARS-CoV-2 at MOI of 5. The immunoblot was probed with anti-TRMT1, actin, or SARS-CoV-2 nucleocapsid (N) antibodies. Circle represents endogenous full-length TRMT1. Asterisk denotes a non-specific band. (B) Quantification of TRMT1 signal intensity normalized to actin in the mock or SARS-CoV-2-infected cell lines. (C) m2,2G levels in small RNAs isolated from MRC5 cells that were either mock-infected or infected with SARS-CoV-2 at MOI of 5 for 24 or 48 hours. m2,2G levels were normalized to guanosine. (D) Levels of the indicated RNA modifications in small RNAs isolated from MRC5 cells that were either mock-infected or infected with SARS-CoV-2 for 24 or 48 hours. RNA modification levels were normalized to guanosine. Y-axis represents the log2 fold change in the levels of the indicated tRNA modification between SARS-CoV-2

infected versus mock-infected MRC5 cells. Samples were measured in triplicate. *$p < 0.05$; **$p<0.01$; ****$p < 0.0001$; ns, non-significant.

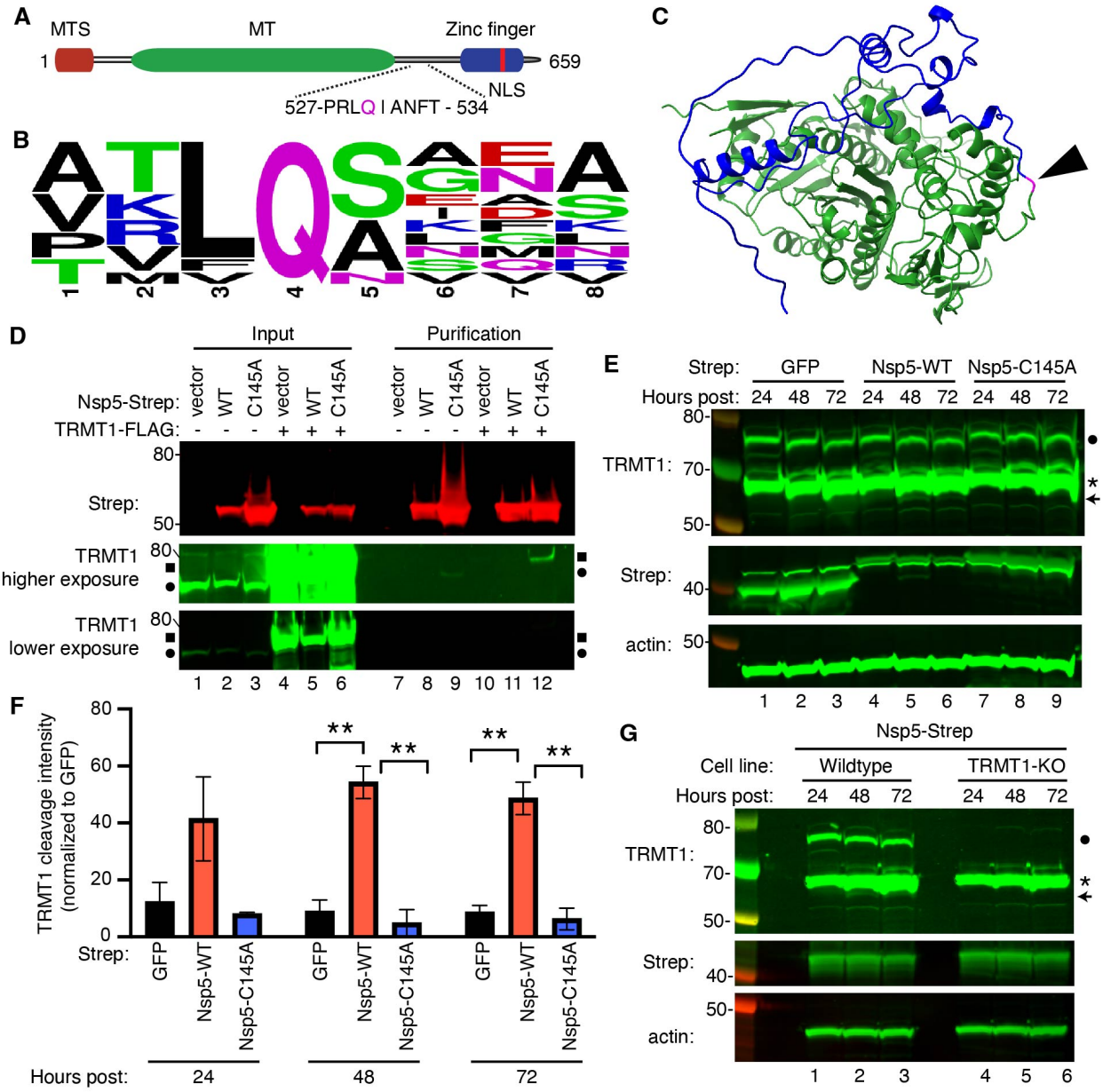

Figure 2. SARS-CoV-2 Nsp5 binds and cleaves TRMT1 in human cells. (A) Schematic of human TRMT1 primary structure with predicted Nsp5 cleavage site. Mitochondrial targeting signal (MTS), methyltransferase (MT) domain and zinc finger motif are denoted. (B) Consensus sequence logo of cleavage sites in SARS-CoV-2 polyproteins. (C) Alpha-fold predicted structure of human TRMT1 with putative Nsp5 cleavage site denoted in magenta and arrowhead. (D) Immunoblot of input and streptactin purifications from human cells expressing empty vector, wildtype (WT) Nsp5, or Nsp5-C145A fused to the Strep tag without or with co-expression with TRMT1-FLAG. The immunoblot was probed with anti-

Strep, FLAG and actin antibodies. Square represents TRMT1-FLAG, circle represents endogenous TRMT1. (E) Immunoblot of lysates prepared from human 293T cells expressing GFP, Nsp5 or Nsp5-C145A. The immunoblot was probed with anti-TRMT1, Strep, actin antibodies. Hours post represents the time post-transfection. Arrow represents the TRMT1 cleavage fragment. * denotes a non-specific band (F) Quantification of TRMT1 cleavage product relative to GFP control transfection in (E). (G) Immunoblot of lysates prepared from wildtype or TRMT1-knockout (KO) human cell lines expressing Nsp5. Experiments in (D) through (G) were repeated three times with comparable results.

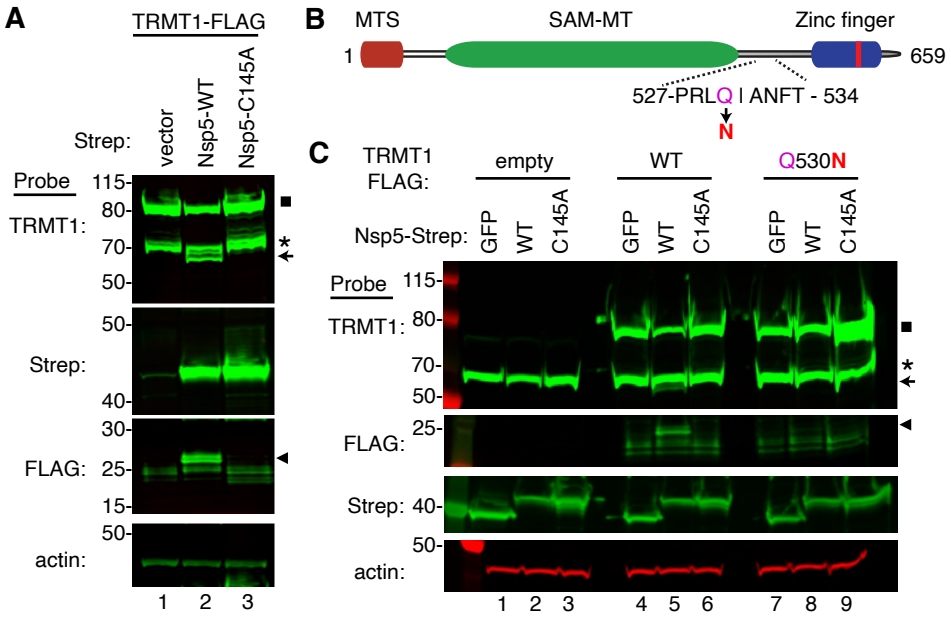

Figure 3. Sequence-dependent cleavage of TRMT1 by SARS-CoV-2 Nsp5. (A) Immunoblot of lysates from human cells expressing empty vector, wildtype (WT) Nsp5-Strep, or Nsp5-C145A-Strep without or with co-expression with TRMT1-FLAG. The immunoblot was probed with anti-Strep, FLAG and actin antibodies. Square represents TRMT1-FLAG, * denotes a non-specific band, arrow represents N-terminal TRMT1 cleavage product and arrowhead indicates the C-terminal TRMT1 cleavage product. (B) Schematic of human TRMT1 with predicted Nsp5 cleavage site and Q530N mutation. (C) Immunoblot of lysates from human cells expressing empty vector, wildtype (WT) Nsp5-Strep, or Nsp5-C145A-Strep without or with co-expression with TRMT1-FLAG or TRMT1-FLAG Q530N. Experiments in (A) and (C) were repeated three times with comparable results.

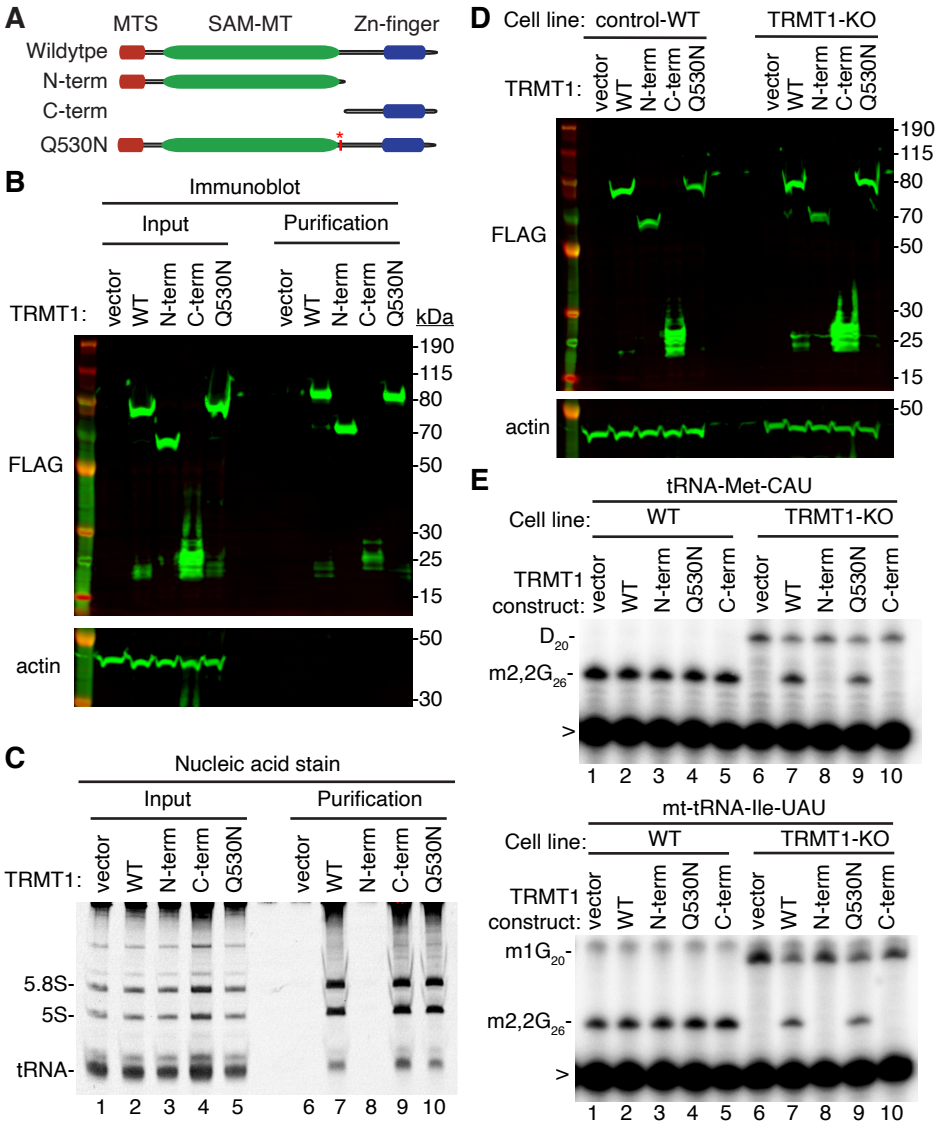

Figure 4. N- and C-terminal TRMT1 cleavage fragments exhibit alterations in RNA binding and tRNA modification activity. (A) Schematic of wildtype TRMT1 and predicted TRMT1 fragments resulting from Nsp5 cleavage at Q530N. (B) Immunoblot analysis of anti-FLAG purifications from human cells expressing vector control, full-length TRMT1, or TRMT1 cleavage fragments fused to the FLAG tag. The immunoblot was probed with anti-FLAG and anti-actin antibodies. (C) Nucleic acid stain of RNAs extracted from the indicated input or purified samples after denaturing PAGE. The migration pattern of 5.8S rRNA (~150 nt), 5S rRNA (~120 nt) and tRNAs (~70–80 nt) are denoted. (D) Immunoblot of TRMT1 expression in either control-WT or TRMT1-KO human 293T cell lines. (E, F) Representative gel

of primer extension assays to monitor the presence of m2,2G in tRNA-Met-CAU or mt-tRNA-Ile-UAU from the cell lines transfected with the indicated TRMT1 constructs. D, dihydrouridine; m1G, 1-methylguanosine; >, labeled oligonucleotide used for primer extension. Protein-RNA purification and primer extension analysis was repeated three times with comparable results.

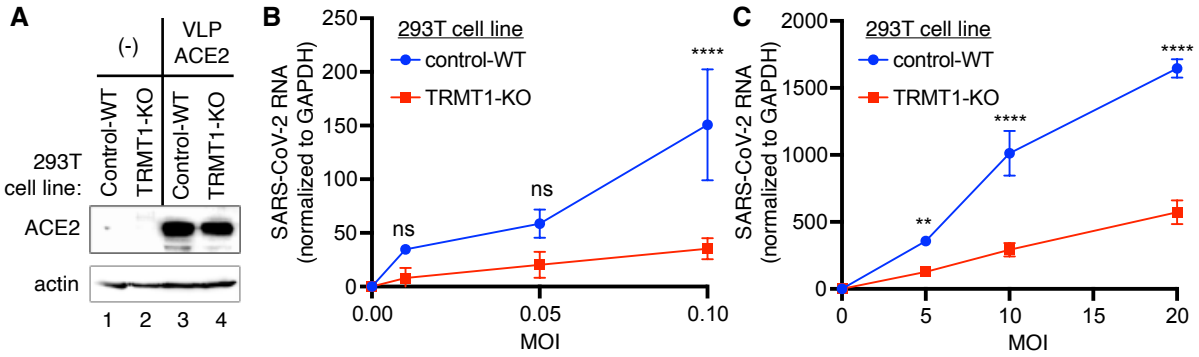

Figure 5. The expression of TRMT1 affects the levels of viral RNA in human cells after infection by SARS-CoV-2. (A) Immunoblot of the indicated 293T cell lines that were uninfected or contain a stable integrated lentiviral vector expressing human ACE2. (B, C) SARS-CoV-2 RNA copy number in control-wildtype (WT) or TRMT1-KO human 293T cell lines after infection at the indicated MOI. Viral copy number was measured by QRT-PCR and normalized to GAPDH. Samples were measured in triplicate. *p < 0.05; **p<0.01; ****p < 0.0001; ns, non-significant.

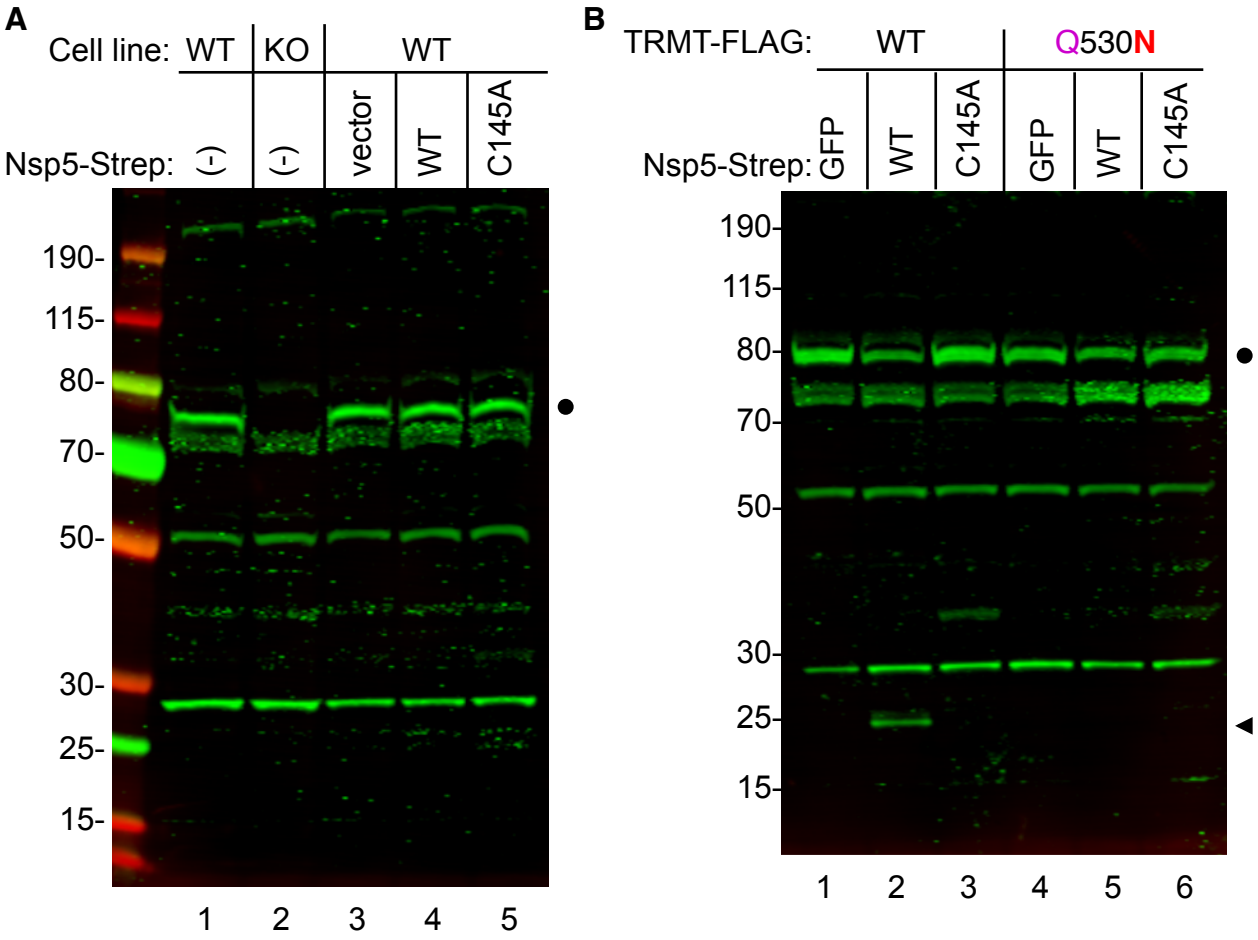

Supplemental Figure 1. Detection of the C-terminal TRMT1 fragment produced by Nsp5-dependent cleavage in human cells. (A) Immunoblot of lysates from the indicated wildtype (WT) or TRMT1-KO human 293T cells that were untransfected (-) (lanes 1 and 2) or transfected with empty vector, wildtype (WT) Nsp5-Strep, or Nsp5-C145A-Strep expression plasmids (lanes 3 through 5). The blot was probed with an antibody detecting residues 609-659 of TRMT1. Circle represents endogenous TRMT1. (B) Immunoblot of lysates from human cells that were transfected with TRMT1-FLAG or TRMT1-FLAG Q530N expression plasmids along with empty vector, wildtype (WT) Nsp5-Strep, or Nsp5-C145A-Strep expression plasmids. The blot was probed with an antibody detecting residues 609-659 of TRMT1. Circle represents endogenous TRMT1 and arrowhead indicates the C-terminal TRMT1 cleavage product.

References

Blaesius K, Abbasi AA, Tahir TH, Tietze A, Picker-Minh S, Ali G, Farooq S, Hu H, Latif Z, Khan MN *et al* (2018) Mutations in the tRNA methyltransferase 1 gene TRMT1 cause congenital microcephaly, isolated inferior vermian hypoplasia and cystic leukomalacia in addition to intellectual disability. *Am J Med Genet A* 176: 2517-2521

Bojkova D, Klann K, Koch B, Widera M, Krause D, Ciesek S, Cinatl J, Munch C (2020) Proteomics of SARS-CoV-2-infected host cells reveals therapy targets. *Nature* 583: 469-472

Burgess HM, Depledge DP, Thompson L, Srinivas KP, Grande RC, Vink EI, Abebe JS, Blackaby WP, Hendrick A, Albertella MR *et al* (2021) Targeting the m(6)A RNA modification pathway blocks SARS-CoV-2 and HCoV-OC43 replication. *Genes Dev* 35: 1005-1019

Cai WM, Chionh YH, Hia F, Gu C, Kellner S, McBee ME, Ng CS, Pang YL, Prestwich EG, Lim KS *et al* (2015) A Platform for Discovery and Quantification of Modified Ribonucleosides in RNA: Application to Stress-Induced Reprogramming of tRNA Modifications. *Methods Enzymol* 560: 29-71

Chen CC, Yu X, Kuo CJ, Min J, Chen S, Ma L, Liu K, Guo RT (2021) Overview of antiviral drug candidates targeting coronaviral 3C-like main proteases. *FEBS J* 288: 5089-5121

Dewe JM, Fuller BL, Lentini JM, Kellner SM, Fu D (2017) TRMT1-Catalyzed tRNA Modifications Are Required for Redox Homeostasis To Ensure Proper Cellular Proliferation and Oxidative Stress Survival. *Mol Cell Biol* 37

Di Giorgio S, Martignano F, Torcia MG, Mattiuz G, Conticello SG (2020) Evidence for host-dependent RNA editing in the transcriptome of SARS-CoV-2. *Sci Adv* 6: eabb5813

Fu D, Brophy JA, Chan CT, Atmore KA, Begley U, Paules RS, Dedon PC, Begley TJ, Samson LD (2010) Human AlkB homolog ABH8 Is a tRNA methyltransferase required for wobble uridine modification and DNA damage survival. *Mol Cell Biol* 30: 2449-2459

Gordon DE, Hiatt J, Bouhaddou M, Rezelj VV, Ulferts S, Braberg H, Jureka AS, Obernier K, Guo JZ, Batra J *et al* (2020a) Comparative host-coronavirus protein interaction networks reveal pan-viral disease mechanisms. *Science* 370

Gordon DE, Jang GM, Bouhaddou M, Xu J, Obernier K, White KM, O'Meara MJ, Rezelj VV, Guo JZ, Swaney DL *et al* (2020b) A SARS-CoV-2 protein interaction map reveals targets for drug repurposing. *Nature* 583: 459-468

Grum-Tokars V, Ratia K, Begaye A, Baker SC, Mesecar AD (2008) Evaluating the 3C-like protease activity of SARS-Coronavirus: recommendations for standardized assays for drug discovery. *Virus Res* 133: 63-73

Heilmann E, Costacurta F, Geley S, Mogadashi SA, Volland A, Rupp B, Harris RS, von Laer D (2022) A VSV-based assay quantifies coronavirus Mpro/3CLpro/Nsp5 main protease activity and chemical inhibition. *Commun Biol* 5: 391

Jin Y, Ouyang M, Yu T, Zhuang J, Wang W, Liu X, Duan F, Guo D, Peng X, Pan JA (2022) Genome-Wide Analysis of the Indispensable Role of Non-structural Proteins in the Replication of SARS-CoV-2. *Front Microbiol* 13: 907422

Jonkhout N, Cruciani S, Santos Vieira HG, Tran J, Liu H, Liu G, Pickford R, Kaczorowski D, Franco GR, Vauti F *et al* (2021) Subcellular relocalization and nuclear redistribution of the RNA methyltransferases TRMT1 and TRMT1L upon neuronal activation. *RNA Biol* 18: 1905-1919

Jumper J, Evans R, Pritzel A, Green T, Figurnov M, Ronneberger O, Tunyasuvunakool K, Bates R, Zidek A, Potapenko A *et al* (2021) Highly accurate protein structure prediction with AlphaFold. *Nature* 596: 583-589

Kim D, Lee JY, Yang JS, Kim JW, Kim VN, Chang H (2020) The Architecture of SARS-CoV-2 Transcriptome. *Cell* 181: 914-921 e910

Lamers MM, Haagmans BL (2022) SARS-CoV-2 pathogenesis. *Nat Rev Microbiol* 20: 270-284

Lee J, Kenward C, Worrall LJ, Vuckovic M, Gentile F, Ton AT, Ng M, Cherkasov A, Strynadka NCJ, Paetzel M (2022) X-ray crystallographic characterization of the SARS-CoV-2 main protease polyprotein cleavage sites essential for viral processing and maturation. *Nat Commun* 13: 5196

Lee J, Worrall LJ, Vuckovic M, Rosell FI, Gentile F, Ton AT, Caveney NA, Ban F, Cherkasov A, Paetzel M *et al* (2020) Crystallographic structure of wild-type SARS-CoV-2 main protease acyl-enzyme intermediate with physiological C-terminal autoprocessing site. *Nat Commun* 11: 5877

Li C, Yao Y, Long D, Lin X (2021a) KDELC1 and TRMT1 Serve as Prognosis-Related SARS-CoV-2 Proteins Binding Human mRNAs and Promising Biomarkers in Clear Cell Renal Cell Carcinoma. *Int J Gen Med* 14: 2475-2490

Li N, Hui H, Bray B, Gonzalez GM, Zeller M, Anderson KG, Knight R, Smith D, Wang Y, Carlin AF *et al* (2021b) METTL3 regulates viral m6A RNA modification and host cell innate immune responses during SARS-CoV-2 infection. *Cell Rep* 35: 109091

Liu Y, Qin C, Rao Y, Ngo C, Feng JJ, Zhao J, Zhang S, Wang TY, Carriere J, Savas AC *et al* (2021) SARS-CoV-2 Nsp5 Demonstrates Two Distinct Mechanisms Targeting RIG-I and MAVS To Evade the Innate Immune Response. *mBio* 12: e0233521

Merad M, Blish CA, Sallusto F, Iwasaki A (2022) The immunology and immunopathology of COVID-19. *Science* 375: 1122-1127

Meyer B, Chiaravalli J, Gellenoncourt S, Brownridge P, Bryne DP, Daly LA, Grauslys A, Walter M, Agou F, Chakrabarti LA *et al* (2021) Characterising proteolysis during SARS-CoV-2 infection identifies viral cleavage sites and cellular targets with therapeutic potential. *Nat Commun* 12: 5553

Meyers JM, Ramanathan M, Shanderson RL, Beck A, Donohue L, Ferguson I, Guo MG, Rao DS, Miao W, Reynolds D *et al* (2021) The proximal proteome of 17 SARS-CoV-2 proteins links to disrupted antiviral signaling and host translation. *PLoS Pathog* 17: e1009412

Moustaqil M, Ollivier E, Chiu HP, Van Tol S, Rudolffi-Soto P, Stevens C, Bhumkar A, Hunter DJB, Freiberg AN, Jacques D *et al* (2021) SARS-CoV-2 proteases PLpro and 3CLpro cleave IRF3 and critical modulators of inflammatory pathways (NLRP12 and TAB1): implications for disease presentation across species. *Emerg Microbes Infect* 10: 178-195

Muramatsu T, Kim YT, Nishii W, Terada T, Shirouzu M, Yokoyama S (2013) Autoprocessing mechanism of severe acute respiratory syndrome coronavirus 3C-like protease (SARS-CoV 3CLpro) from its polyproteins. *FEBS J* 280: 2002-2013

Najmabadi H, Hu H, Garshasbi M, Zemojtel T, Abedini SS, Chen W, Hosseini M, Behjati F, Haas S, Jamali P *et al* (2011) Deep sequencing reveals 50 novel genes for recessive cognitive disorders. *Nature* 478: 57-63

Narayanan A, Toner SA, Jose J (2022) Structure-based inhibitor design and repurposing clinical drugs to target SARS-CoV-2 proteases. *Biochem Soc Trans* 50: 151-165

Nie X, Qian L, Sun R, Huang B, Dong X, Xiao Q, Zhang Q, Lu T, Yue L, Chen S *et al* (2021) Multi-organ proteomic landscape of COVID-19 autopsies. *Cell* 184: 775-791 e714

Owen DR, Allerton CMN, Anderson AS, Aschenbrenner L, Avery M, Berritt S, Boras B, Cardin RD, Carlo A, Coffman KJ *et al* (2021) An oral SARS-CoV-2 M(pro) inhibitor clinical candidate for the treatment of COVID-19. *Science* 374: 1586-1593

Pallan PS, Kreutz C, Bosio S, Micura R, Egli M (2008) Effects of N2,N2-dimethylguanosine on RNA structure and stability: crystal structure of an RNA duplex with tandem m2 2G:A pairs. *RNA* 14: 2125-2135

Peng X, Luo Y, Li H, Guo X, Chen H, Ji X, Liang H (2022) RNA editing increases the nucleotide diversity of SARS-CoV-2 in human host cells. *PLoS Genet* 18: e1010130

Perez M, Nance KD, Bak DW, Thalalla Gamage S, Najera SS, Conte AN, Linehan WM, Weerapana E, Meier JL (2022) Conditional Covalent Lethality Driven by Oncometabolite Accumulation. *ACS Chem Biol* 17: 2789-2800

Pettersen EF, Goddard TD, Huang CC, Couch GS, Greenblatt DM, Meng EC, Ferrin TE (2004) UCSF Chimera--a visualization system for exploratory research and analysis. *J Comput Chem* 25: 1605-1612

Ramos J, Han L, Li Y, Hagelskamp F, Kellner SM, Alkuraya FS, Phizicky EM, Fu D (2019) Formation of tRNA Wobble Inosine in Humans Is Disrupted by a Millennia-Old Mutation Causing Intellectual Disability. *Molecular and cellular biology* 39

Raymonda MH, Ciesla JH, Monaghan M, Leach J, Asantewaa G, Smorodintsev-Schiller LA, Lutz MMt, Schafer XL, Takimoto T, Dewhurst S *et al* (2022) Pharmacologic profiling reveals lapatinib as a novel antiviral against SARS-CoV-2 in vitro. *Virology* 566: 60-68

Samavarchi-Tehrani P, Abdouni H, Knight JDR, Astori A, Samson R, Lin Z-Y, Kim D-K, Knapp JJ, St-Germain J, Go CD *et al* (2020) A SARS-CoV-2 – host proximity interactome. *bioRxiv*: 2020.2009.2003.282103

Schmidt TG, Batz L, Bonet L, Carl U, Holzapfel G, Kiem K, Matulewicz K, Niermeier D, Schuchardt I, Stanar K (2013) Development of the Twin-Strep-tag(R) and its application for purification of recombinant proteins from cell culture supernatants. *Protein Expr Purif* 92: 54-61

Steinberg S, Cedergren R (1995) A correlation between N2-dimethylguanosine presence and alternate tRNA conformers. *RNA* 1: 886-891

Uemura K, Nobori H, Sato A, Sanaki T, Toba S, Sasaki M, Murai A, Saito-Tarashima N, Minakawa N, Orba Y *et al* (2021a) 5-Hydroxymethyltubercidin exhibits potent antiviral activity against flaviviruses and coronaviruses, including SARS-CoV-2. *iScience* 24: 103120

Uemura K, Sasaki M, Sanaki T, Toba S, Takahashi Y, Orba Y, Hall WW, Maenaka K, Sawa H, Sato A (2021b) MRC5 cells engineered to express ACE2 serve as a model system for the discovery of antivirals targeting SARS-CoV-2. *Sci Rep* 11: 5376

V'Kovski P, Kratzel A, Steiner S, Stalder H, Thiel V (2021) Coronavirus biology and replication: implications for SARS-CoV-2. *Nat Rev Microbiol* 19: 155-170

Varadi M, Anyango S, Deshpande M, Nair S, Natassia C, Yordanova G, Yuan D, Stroe O, Wood G, Laydon A *et al* (2022) AlphaFold Protein Structure Database: massively expanding the structural coverage of protein-sequence space with high-accuracy models. *Nucleic Acids Res* 50: D439-D444

Wenzel J, Lampe J, Muller-Fielitz H, Schuster R, Zille M, Muller K, Krohn M, Korbelin J, Zhang L, Ozorhan U *et al* (2021) The SARS-CoV-2 main protease M(pro) causes microvascular brain pathology by cleaving NEMO in brain endothelial cells. *Nat Neurosci* 24: 1522-1533

Yan S, Wu G (2021) Spatial and temporal roles of SARS-CoV PL(pro) -A snapshot. *FASEB J* 35: e21197

Zhang J, Cruz-Cosme R, Zhuang MW, Liu D, Liu Y, Teng S, Wang PH, Tang Q (2020a) A systemic and molecular study of subcellular localization of SARS-CoV-2 proteins. *Signal Transduct Target Ther* 5: 269

Zhang K, Lentini JM, Prevost CT, Hashem MO, Alkuraya FS, Fu D (2020b) An intellectual disability-associated missense variant in TRMT1 impairs tRNA modification and reconstitution of enzymatic activity. *Hum Mutat* 41: 600-607

Zhang LS, Xiong QP, Pena Perez S, Liu C, Wei J, Le C, Zhang L, Harada BT, Dai Q, Feng X *et al* (2021a) ALKBH7-mediated demethylation regulates mitochondrial polycistronic RNA processing. *Nat Cell Biol* 23: 684-691

Zhang S, Wang J, Cheng G (2021b) Protease cleavage of RNF20 facilitates coronavirus replication via stabilization of SREBP1. *Proc Natl Acad Sci U S A* 118

Zhang X, Hao H, Ma L, Zhang Y, Hu X, Chen Z, Liu D, Yuan J, Hu Z, Guan W (2021c) Methyltransferase-like 3 Modulates Severe Acute Respiratory Syndrome Coronavirus-2 RNA N6-Methyladenosine Modification and Replication. *mBio* 12: e0106721